Demonstration of reconfigurable optical generation of higher-order modulation formats up to 64 QAM using optical nonlinearity

Mohammad Reza Chitgarha,[1,*] Salman Khaleghi,[1] Zahra Bakhtiari,[1] Morteza Ziyadi,[1] Ori Gerstel,[2] Loukas Paraschis,[2] Carsten Langrock,[3] Martin M. Fejer,[3] and Alan E. Willner[1]

[1]*Department of Electrical Engineering, University of Southern California, Los Angeles, California 90089, USA*

[2]*Cisco Systems, Inc., 170 West Tasman Dr., San Jose, California 95134, USA*

[3]*Edward L. Ginzton Laboratory, Stanford University, Stanford, California 94305, USA*

**Corresponding author: chitgarh@usc.edu*

Received June 27, 2013; accepted July 28, 2013;
posted August 7, 2013 (Doc. ID 192997); published August 26, 2013

We demonstrate a reconfigurable optical transmitter of higher-order modulation formats including pulse-amplitude-modulation (PAM) signals and quadrature-amplitude-modulation (QAM) signals. We generated six different modulation formats by multiplexing 10 Gbit/s on–off-keying (OOK) signals (10 Gbaud binary phase-shift keying, 4-PAM, 8-PAM quadrature phase-shift keying (QPSK), 16-QAM and 16-star-QAM with error-vector magnitudes (EVMs) of 8.1%, 7.5%, 7.8%, 8.2%, 7.2%, and 6.9%, respectively) and 80 Gbit/s 16-QAM with an EVM of 8.5%, as well as 120 Gbit/s 64-QAM with an EVM of 7.1%, using two or three 40 Gbit/s QPSK signals, respectively. We also successfully transmitted the generated 16-QAM signals through a 100 km transmission line with negligible power penalty.

OCIS codes: (060.2360) Fiber optics links and subsystems; (060.4370) Nonlinear optics, fibers; (190.4223) Nonlinear wave mixing.
http://dx.doi.org/10.1364/OL.38.003350

Dramatic growth of data capacity demand in optical networks has necessitated an increase in the data speeds of terminal transmitters [1,2]. Due to the finite bandwidth over the C- and L-bands in a single core fiber, utilizing spectrally efficient higher-order modulation formats for the data channels has raised much research interest as a candidate for scaling up the aggregate capacity [1–3]. A laudable goal would be to have a reconfigurable transmitter capable of generating higher-order modulation formats for 16-quadrature amplitude modulation (QAM) and beyond [2].

A common technique for generating higher-order formats is to use electronic circuits to drive an in-phase quadrature (IQ) modulator by multilevel electrical signals [4,5]. However, because of the limited linearity, cost, and complexity of the electronics at higher baud rates, this method might become dramatically difficult at rates exceeding 50 Gbauds. Another approach is to use integrated parallel modulators to synthesize an optically higher-order QAM signal with lower complexity in driving electronics [3,6]. On the other hand, the tandem-modulator approach, in which two IQ modulators with a dual-drive Mach–Zehnder modulator are cascaded together, can reduced the complexity in driving electronics [7].

One potential approach to achieving a higher-order QAM transmitter is the use of optical nonlinearities to perform reconfigurable multiplexing of different data channels with lower-order QAM to a single data channel with higher-order QAM. Wave mixing using nonlinearities may have bandwidths of the order of terahertz or greater as well as transparency to the data bit rate and modulation format. Previously, methods for higher-order QAM generation using nonlinearities include multiplexing of two 10 Gbaud quadrature phase-shift keying (QPSK) signals to a 10 Gbaud 16-star-QAM [8] and multiplexing four on–off-keying (OOK) signals into 16-QAM by employing a nonlinear optical loop mirror [9]. In general, these methods tend not to be readily tunable over the various parameters, such as bit rates and data modulation formats.

In this Letter, we demonstrate a reconfigurable optical generation of higher-order modulation formats including pulse-amplitude-modulation (PAM) signals and QAM signals. We generated six different modulation formats by multiplexing 10 Gbit/s OOK signals [10 Gbaud binary phase-shift keying (BPSK), 4-PAM, 8-PAM, QPSK, 16-QAM, and 16-star-QAM] and 80 Gbit/s 16-QAM with an error-vector magnitude (EVM) of 8.5%, as well as 120 Gbit/s 64-QAM with an EVM of 7.1% using two or three 40 Gbit/s QPSK signals, respectively. We also successfully transmitted the generated 16-QAM signals through a 100 km transmission line with a negligible power penalty.

The principle operation of our proposed optical higher-order QAM transmitter is shown in Fig. 1. First, multiple IQ modulators are used to modulate lower-order QAM on multiple continuous wave (CW) lasers with different wavelengths. Then, a nonlinear wave mixer generates a phase conjugate copy of each input signal by using an injected CW laser pump. A liquid-crystal-on-silicon (LCoS) programmable filter is used to apply complex weights on the signals. Subsequently, a dispersive element induces a relative delay between each signal and its corresponding conjugate copy. Finally, another nonlinear element is utilized to mix each signal, its phase conjugate copy, and another injected signal in order to coherently multiplex the lower-order QAM signals to a higher-order QAM signal [10,11].

In our proposed scheme, periodically poled lithium-niobate (PPLN) waveguides are used for creating phase conjugate copies of the original signals and also for

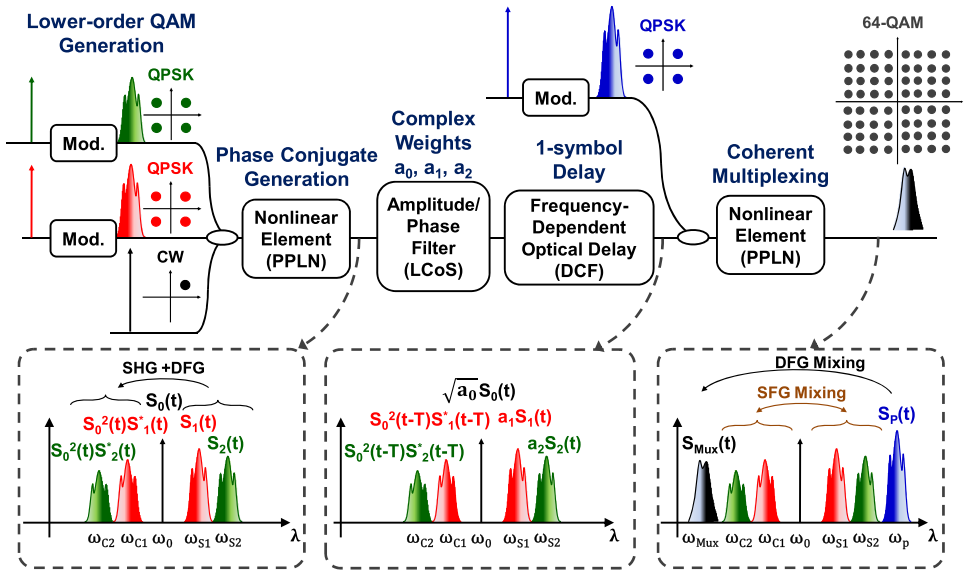

Fig. 1. Conceptual block diagram of a reconfigurable optical QAM transmitter.

realizing coherent multiplexing. A conversion–dispersion-based delay is realized in a spool of dispersion-compensating fiber (DCF) to induce a relative delay between each signal and its replica [12,13].

In the first PPLN waveguide, the CW pump laser with electric field $S_0(t)$, located at quasi-phase-matching wavelength ω_0, is mixed with itself through second-harmonic-generation (SHG), which creates the mixing term $S_0^2(t)$ at $2\omega_0$. The SHG term then mixes with multiple input signals at frequencies ω_{Si} through difference-frequency-generation (DFG) nonlinear processes to create phase conjugate replicas at $2\omega_0 - \omega_{si}$. Given that the electric field of each input signal is $S_i(t)$, the electric field of the generated signal is proportional to $S_0^2(t) \times S_i^*(t)$.

The output of the first PPLN waveguide is sent into an amplitude- and phase-programmable filter (based on LCoS technology) followed by a frequency-dependent optical delay element (i.e., a DCF spool), in which (i) the input signals and their corresponding phase conjugate copies as well as the CW pump laser are filtered, (ii) the complex weights a_i are applied to them, and (iii) a relative delay (T) between each signal and its corresponding conjugate copy is induced. Therefore, the electric fields of the signals, their phase conjugate replicas, and the CW pump become $a_i S_i(t)$, $S_0^2(t-T) \times S_i^*(t-T)$, and $\sqrt{a_0}S_0(t)$, respectively.

In the multiplexing stage, each signal $S_i(t)$ at ω_{Si} and its corresponding delayed replica, which are located symmetrically around ω_0, are mixed through sum-frequency generation in the second PPLN waveguide with the same quasi-phase-matching wavelength, and they generate a new signal with an electric field of

$$X_i(t) \triangleq S_0^2(t) \times S_i(t) \times S_i^*(t-T) \tag{1}$$

at $2\omega_0$. The challenge in realizing multiplexing of X_i lies in the fact that these signals need to be coherent. As the time delay between signal and its conjugate copy are significantly smaller than the inverse of the laser line widths, $\nu_i's$ (i.e., $T \ll 1/\nu_i$), the residual phase noises of $S_i(t) \times S_i^*(t-T)$ are negligible and are dominated by the phase noise of $S_0^2(t)$ for all X_i. Therefore, although the input signals S_i are generated separately from different lasers with different phase noises (i.e., non-phase-locked sources), all signals after mixing with their corresponding delayed copies are phase locked to $S_0^2(t)$ and can be coherently multiplexed at $2\omega_0$. The SHG term of the CW signal, i.e., $X_0(t) \triangleq S_0^2(t)$, is also combined coherently with X_i. Another signal at ω_P with electric field $S_P(t)$ is also injected to the second PPLN waveguide for the DFG nonlinear process to convert the multiplexed signal to frequency $\omega_{\text{Mux}} \triangleq 2\omega_0 - \omega_P$. Hence, the electric field of the generated signal at ω_{Mux} can be expressed as

$$S_{\text{Mux}}(t) = S_p^*(t) \times \sum_{i=1}^{N} a_i X_i(t), \tag{2}$$

in which the complex coefficient (a_i), the number of input signals (N), and the delay between signals and their corresponding conjugate copies (T) can be tuned to generate different signals. Therefore the electrical data streams encoded on S_i, which can eventually generate X_i, with lower-order QAM formats (OOK, or QPSK), create a higher-order QAM (e.g., 16-QAM, 16-star-QAM, or 64-QAM) according to Eq. (2).

For OOK signals, the delay is set to 0 and thus $X_i(t) = S_0^2(t) \times |S_i(t)|^2$. Both $S_i(t)$ and $|S_i(t)|^2$ carry the same data bits, because the S_i are modulated with OOK symbols (i.e., 0 or 1). Figure 2(a) shows multiplexing of four OOK signals and a CW pump to create a 16-QAM signal. As can be seen, the constant vector (i.e., CW pump) and four OOK symbols are scaled by $a_0 = -1.5 - 1.5j$, $a_1 = 1$, $a_2 = 0.5$, $a_3 = j$, and $a_4 = 0.5j$, respectively, and combined in the complex plane.

For the phase-modulated signal, on the other hand, as the data is encoded on the phase of its electric field, the product of the signal and its corresponding phase conjugate does not contain any data pattern. Therefore, a one-symbol relative delay, T_S, is induced between S_i and S_i^*

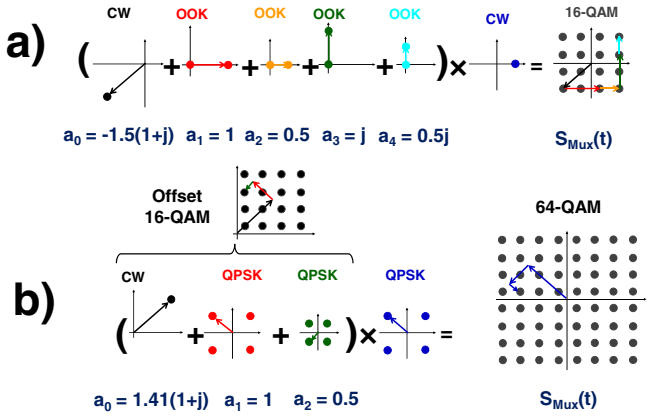

Fig. 2. Generating (a) 16- and (b) 64-QAM signals using four OOK signals and three QPSK signals, respectively.

before the mixing process occurs. In this case, $X_i(t) = S_0^2(t) \times S_i(t) \times S_i^*(t - T_S)$, in which the phase of the data symbols, $\varphi_{X_i}(t)$, are equal to the differential version of the input symbols phases [i.e., $\varphi_{X_i}(t) = \varphi_{Si}(t) - \varphi_{Si}(t - T_S)$]. This fact needs to be taken into consideration for the encoding of $S_i(t)$ to obtain the desired signal at the output. Figure 2(b) shows the generation of a 64-QAM signal using three QPSK signals. First, a CW pump laser and two QPSK signals [$X_0(t)$, $X_1(t)$, and $X_2(t)$] are combined with a complex coefficient of $a_0 = 1.41 + 1.41j$, $a_1 = 1$, and $a_2 = 0.5$ to create an offset-16-QAM in the upper right-hand quadrant of the IQ plane. Then this signal is mixed with another QPSK and mapped to the other quadrants to complete the 64-QAM constellation points.

The experimental setup of the optical QAM transmitter is depicted in Fig. 3. First, four CW lasers at wavelengths $\lambda_{S1-4} =$ of 1551.8, 1553.4, 1555, and 1556.6 nm are coupled and sent into nested Mach–Zehnder modulators

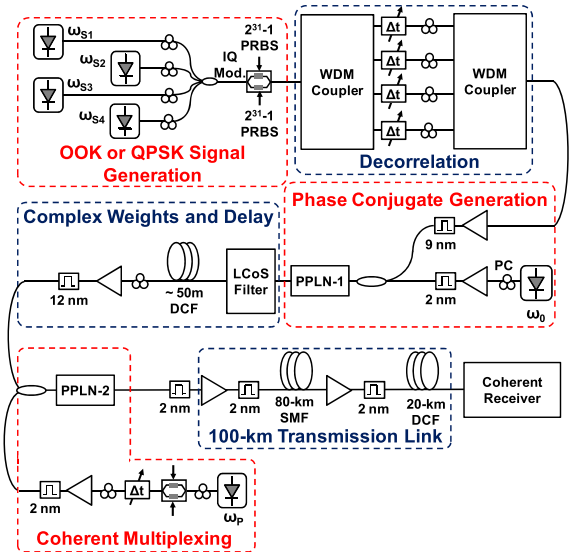

PM: Phase Modulator
MZM: Mach-Zender Modulator
DCF: Dispersion compensating fiber
PC: Polarization controller
DLI: Delay Line Interferometer
BPF: Bandpass Filter

Fig. 3. Experimental setup for the proposed optical QAM transmitter. PM, phase modulator; PC, polarization controller; MZM, Mach–Zehnder modulator; DLI, delay-line interferometer; DCF, dispersion-compensating fiber; BPF, bandpass filter.

driven by 10 or 20 Gbit/s pseudorandom bit sequences $2^{31} - 1$ to generate four 10 Gbit/s OOK or 40 Gbit/s QPSK signals (lower-order QAMs). In order to decorrelate the input signals, they are separated and independently delayed by use of a WDM coupler and four tunable delay lines, respectively. These signals are then combined in another WDM coupler, amplified, coupled by an amplified CW pump laser at $\lambda_0 = 1549.5$ nm, and injected into the first PPLN waveguide. The CW pump interacts with all input signals through cascaded SHG and DFG nonlinear processes and generates the phase conjugate replicas of the input signals at $\lambda_{C1-4} = 1542.2$, 1545.8, 1547.4, and 1549 nm. The PPLN-1 output is then sent to an LCoS programmable filter in which the CW pump laser, the signals, and their corresponding conjugate copies are filtered with appropriate complex weights. For the QPSK signals, the LCoS output is also passed through a spool of DCF of length ~50 m to induce a one-symbol delay between the signals and their corresponding copies. The LCoS filter is used to induce partial delays to ensure an exactly one-symbol delay for all signals. Subsequently, theses signals are amplified and filtered altogether and sent to another PPLN waveguide. Another CW pump laser (or a modulated signal) at $\lambda_p =$ 1558.2 nm is also injected into PPLN-2 after synchronization with the input signals and sufficient amplification. In the second PPLN, the input signals mix with their corresponding replicas and the injected pump and are multiplexed coherently at $\lambda_{\text{Mux}} = 1540.8$ nm. This signal is then filtered and sent to a transmission link of length 100 km, which consists of two erbium-doped fiber amplifiers, 80 km SMF-28, and 20 km DCF. The output of the transmission link is finally sent to a coherent receiver to record and measure the constellation, the bit-error rate (BER), and the EVM of the output signal.

Coherent multiplexing of multiple OOK signals with different complex coefficients is depicted in Fig. 4. The optical spectra of PPLN-1 and PPLN-2 outputs are shown in Figs. 4(a) and 4(b) when four OOK signals along with a CW pump laser are multiplexed together to generate a 16-QAM signal. In the first PPLN waveguide, the phase conjugate copies of the OOK signals are generated by using the CW pump laser, whereas in the second PPLN waveguide these signals mix with their corresponding phase conjugate replicas and are multiplexed coherently together, and also with the CW pump laser, to generate a higher-order QAM. Figures 4(c)–4(h) show different signals with higher-order modulation formats generated from multiple OOK signals when they are scaled with different complex coefficients and combined coherently. In Fig. 4(c), an OOK signal is converted to a BPSK signal by multiplexing it coherently with a CW pump laser when $a_1 = 1$ and $a_0 = -0.5$. Figure 4(d) shows in-phase multiplexing of two OOK signals with $a_1 = 1$ and $a_2 = 0.5$ along with a CW signal with $a_0 = 1.5$ to generate a 4-PAM signal. In Fig. 4(e), a CW pump laser and three OOK signals with $a_0 = 1.75$, $a_1 = 1$, $a_2 = 0.5$, and $a_3 = 0.25$ are used to generate an 8-PAM signal. In Fig. 4(f), a CW pump laser and two OOK signals with the same amplitudes and $\pi/2$ phase shift are multiplexed coherently (i.e., $a_0 = -0.5 + -0.5j$, $a_1 = 1$, and $a_0 = j$) to generate a QPSK signal. A CW signal and four OOK signals are multiplexed

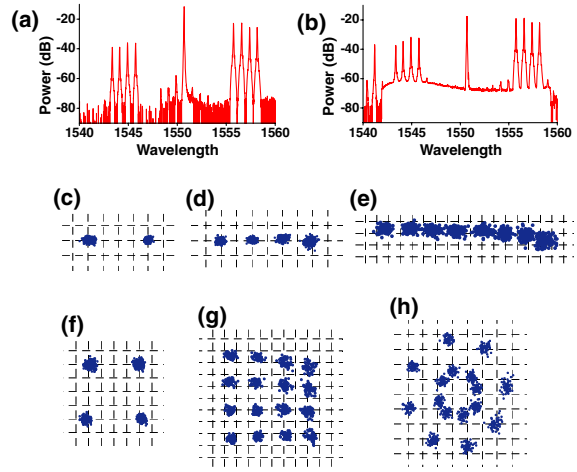

Fig. 4. Higher-level modulation format generation using OOK signals. Optical spectra of (a) phase conjugate copy generation stage (PPLN-1 output) and (b) multiplexing stage (PPLN-2 output). Optical constellation diagrams of (c) 10 Gbit/s BPSK, (d) 20 Gbit/s 4-PAM, (e) 30 Gbit/s 8-PAM, (f) 20 Gbit/s QPSK, (g) 40 Gbit/s 16-QAM, and (h) 40 Gbit/s 16-star-QAM with EVMs of 8.1%, 7.5%, 7.8%, 8.2%, 6.9%, and 6.4%, respectively.

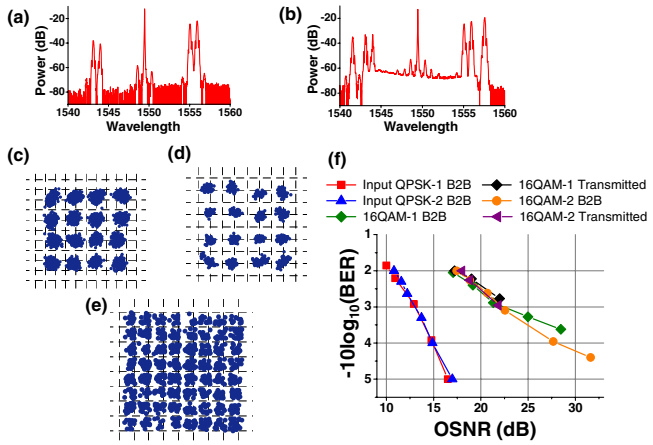

Fig. 5. Higher-level modulation format generation using QPSK signals. Optical spectra of (a) the phase conjugate copy generation stage (PPLN-1 output) and (b) the multiplexing stage (PPLN-2 output). Optical constellation diagrams of generated (c) 80 Gbit/s 16-QAM with multiplexing of two QPSK signals, (d) 80 Gbit/s 16-QAM with multiplexing of a QPSK signal with a CW pump and mixing with another QPSK signal, and (e) 120 Gbit/s 64-QAM with EVMs of 9.1%, 8.5%, and 7.1%. (f) BER measurements of the back-to-back (B2B) signals and the transmitted signals.

coherently to generate, first, a 16-QAM when $a_0 = -1.5 - 1.5j$, $a_1 = 1$, $a_2 = 0.5$, $a_3 = j$, and $a_4 = 0.5j$, and then a 16-star-QAM when $a_0 = -0.75 - 0.75j$, $a_1 = 1 + j$, $a_2 = 1 - j$, $a_3 = -1 + j$, and $a_4 = -1 - j$, which are shown in Figs. 4(g) and 4(h), respectively.

Figure 5 shows coherent multiplexing of multiple QPSK signals to 16- and 64-QAM signals. The spectrum of PPLN-1 output, in which a CW pump laser generates phase conjugate copies of two QPSK signals, is shown in Fig. 5(a). Figure 5(b) shows the spectrum of the second PPLN waveguide and how these signals are coherently multiplexed together and mix with another QPSK signal. Figures 5(c) and 5(d) show two 16-QAM signals with two different generation methods. In the first method, two QPSK signals with $a_1 = 1$ and $a_2 = 0.5$ are multiplexed together and mixed with a CW pump laser [Fig. 5(d)]. In the second method, however, a CW pump laser and a QPSK signal are multiplexed together to generate an offset QPSK, which is mapped to the upper right-hand quadrant of the IQ complex plane with $a_0 = 1.5 + 1.5j$ and $a_1 = 1$. This signal is mixed with another QPSK signal to generate all 16-QAM constellation points. The EVM of the latter 16-QAM is considerably better than the former one. The lower coefficient of the second QPSK signal in the first method can result in lower quality in the generated signal. Figure 5(e) shows the optical constellation of the output 64-QAM signal when $a_0 = 1.41 + 1.41j$, $a_1 = 1$, and $a_2 = 0.5$.

The BER measurements have been performed to quantify the quality of the generated signals. Figure 5(f) shows the BER curves for two input QPSK signals and the generated 16-QAM with two different methods before and after the transmission through 80 km of SMF-28 and 20 km of DCF. For both methods, the power penalties are negligible after 100 km transmission.

This work was made possible by support from NSF, CIAN, DARPA, and Cisco Systems.

References

1. A. H. Gnauck, P. J. Winzer, A. Konczykowska, F. Jorge, J.-Y. Dupuy, M. Riet, G. Charlet, B. Zhu, and D. W. Peckham, J. Lightwave Technol. **30**, 532 (2012).
2. G. Li, Adv. Opt. Photon. **1**, 279 (2009).
3. A. Sano, T. Kobayashi, K. Ishihara, H. Masuda, S. Yamamoto, K. Mori, E. Yamazaki, E. Yoshida, Y. Miyamoto, T. Yamada, and H. Yamazaki, in *European Conference on Optical Communication (ECOC)* (2010), paper PD2.4.
4. Y. Koizumi, K. Toyoda, M. Yoshida, and M. Nakazawa, Opt. Express **20**, 12508 (2012).
5. R. Schmogrow, D. Hillerkuss, M. Dreschmann, M. Huebner, M. Winter, J. Meyer, B. Nebendahl, C. Koos, J. Becker, W. Freude, and J. Leuthold, IEEE Photon. Technol. Lett. **22**, 1601 (2010).
6. T. Sakamoto and A. Chiba, IEEE J. Sel. Top. Quantum Electron. **16**, 1140 (2010).
7. G.-W. Lu, T. Sakamoto, and T. Kawanishi, Opt. Express **21**, 6213 (2013).
8. X. Wu, J. Wang, H. Huang, and A. E. Willner, in *Conference on Lasers and Electro-Optics* (2011), paper CThH4.
9. G. Huang, Y. Miyoshi, A. Maruta, Y. Yoshida, and K.-I. Kitayama, J. Lightwave Technol. **30**, 1342 (2012).
10. Z. Bakhtiari, M. R. Chitgarha, S. Khaleghi, M. Ziyadi, Z. Ma, L. Paraschis, C. Langrock, M. M. Fejer, R. Hellwarth, and A. E. Willner, in *Conference on Lasers and Electro-Optics* (2012), paper CTh1H.3.
11. M. R. Chitgarha, S. Khaleghi, Z. Ma, M. Ziyadi, O. Gerstel, L. Paraschis, C. Langrock, M. Fejer, and A. Willner, in *European Conference on Optical Communication (ECOC)* (2012), paper P3.14.
12. Y. Dai, Y. Okawachi, A. C. Turner-Foster, M. Lipson, A. L. Gaeta, and C. Xu, Opt. Express **18**, 333 (2010).
13. S. Khaleghi, O. F. Yilmaz, M. R. Chitgarha, M. Tur, N. Ahmed, S. Nuccio, I. Fazel, X. Wu, M. W. Haney, C. Langrock, M. M. Fejer, and A. E. Willner, IEEE Photon. J. **4**, 1220 (2012).